Photolytic Reactors: Similitude in Taylor–Couette and Channel Flows

L. J. Forney
School of Chemical Engineering, Georgia Tech, Atlanta, GA 30332

J. A. Pierson
Georgia Tech Research Institute, Atlanta, GA 30332

A similarity law is proposed for the yield from laminar photolytic reactors. In particular, the yield from a fast photolytic reaction is considered in the following three distinctly different reactor geometries: a square channel, an annular gap between concentric cylinders, and Taylor−Couette flow. The similarity law, based on the assumption of a self-similar product concentration profile, demonstrates that the reaction rate can best be described with either zero (small λ) or first-order (large λ) kinetics. Here, the distinction between both cases is determined by the radiation penetration depth, λ. Other geometric parameters affecting scale-up are also discussed.

Introduction

In primary photochemical reactions the electromagnetic energy measured in units of quanta is absorbed by the reacting species, that is, one quantum per molecule. The fate of the excited molecule leads to a number of possible secondary processes, such as fragmentation or elevated electron states, that can promote further chemical reactions (Congdine, 1976).

Such processes, for example, are termed photosynthesis if the absorption occurs in a photosynthetic organism such as unicellular algal (Miller et al., 1964). Another diverse example is the illumination of aqueous, semiconductor photocatalyst powders, which is termed heterogeneous photocatalysis (Ollis and Turchi, 1990; Sczechowski et al., 1995). Photochemical reactions in the field of polymer processing, for example, with vinyl monomers, is yet another example sometimes called photopolymerization (Oster and Yang, 1968). Finally, there is much interest in the field of ultraviolet photobiology with applications in the field of disinfection (Jagger, 1967).

The photochemical processing of liquids independent of the application requires radiation absorption through transparent reactor walls. The efficiency of such processes for a particular photolytic reaction is determined by the distribution of radiation, the fluid residence time, and the hydrodynamics of the flow (Blatchley et al., 1995). The earliest attempts to model photolytic reactors appear to be in the field of photobiology with applications in disinfection. Cortelyou et al. (1954) reported an increase in photoefficiency by increasing turbulence in a continuous flow reactor. Luckiesh and Holladay (1944), Oliver and Cosgrove (1975), and Severin et al. (1984) modeled ideal photolyic reactors as either batch, plug flow, or completely mixed designs with rate constants that are first order with respect to both concentration and radiation intensity. A model for nonideal reactors was developed for Scheible (1987).

More recently, modern CFD computational methods were used to provide a more complete description of the hydrodynamics, and the results were coupled with a number of radiation-intensity models to predict the inactivation of various pathogens (Janex et al., 1998; Blatchley et al., 1998; Lyn et al., 1999). Reasonable agreement was achieved between the CFD computations and the measured inactivation of the pathogens (Chiu et al., 1999). In the latter work, finite rate, first-order kinetics were assumed in turbulent flow for the inactivation of the organisms. The simulated geometries positioned the lamps either parallel or perpendicular (that is, tube bank flow) to the mean fluid velocity for both closed and open channel flows.

In this article we consider the production of triiodide by the fast UV photolysis of iodide. The geometries considered are laminar flow in the following three markedly different reactors: a square channel, an annular gap between concentric cylinders, and Taylor−Couette flow. The latter case con-

Correspondence concerning this article should be addressed to L. J. Forney.

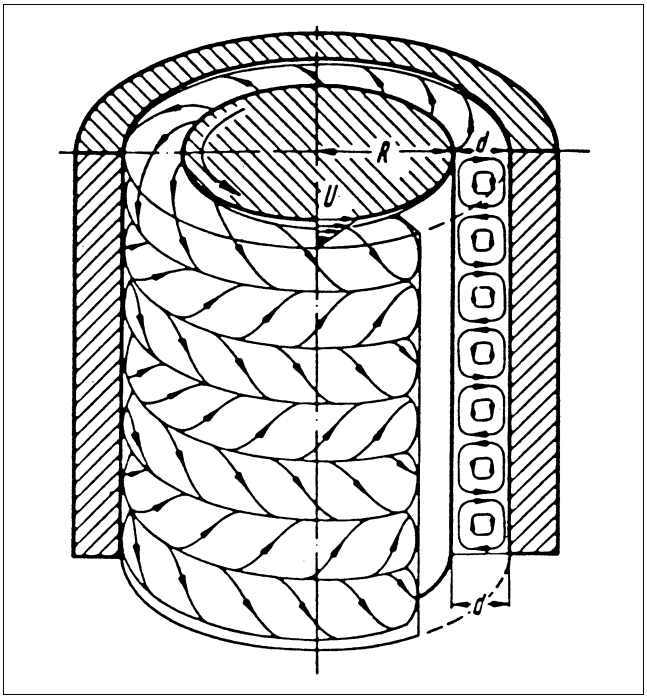

Figure 1. Taylor vortices between two concentric cylinders: inner cylinder rotating, outer cylinder at rest; d–width of annular gap (Schlichting, 1979).

stitutes an example of a spatially periodic flow, as shown in Figure 1, that is similar in many respects to a tube bank (Taylor, 1923; Baier et al., 1999).

Experimental measurements are presented for a variety of reactor flow rates, lamp configurations, and inlet reactant concentrations. The results are correlated with a proposed similarity law that assumes that the product concentration is best described by a self-similar profile within the reactor.

Photochemistry

The reaction used in the present study is the fast UV photolysis of aqueous iodide, producing triiodide. Concentrated KI solutions are optically opaque at wavelengths of 254 nm and act as photon counters (Rahn, 1999). UV absorption by iodide leads to an aqueous or solvated electron via a charge transfer-to-solvent reaction and the formation of an excited iodine atom. The essential reactions are listed below.

$$I^- + h\upsilon \rightarrow I^* + e^- \quad (1)$$

$$I^* + e^- \rightarrow I^- \quad (2)$$

$$2I^* + I^- \rightarrow I_3^- \quad (3)$$

As noted, the UV-induced formation of triiodide is potentially limited by the back reaction of Eq. 2. The quantum yield for triiodide is significantly increased, however, by the addition of potassium iodate. In the presence of iodate, scavenging of the bulk electron occurs, and the following additional reaction is proposed (Rahn, 1997)

$$IO_3^- + e^- + 2H_2O \rightarrow IO^- + H_2O_2 + OH^* + OH^- \quad (4)$$

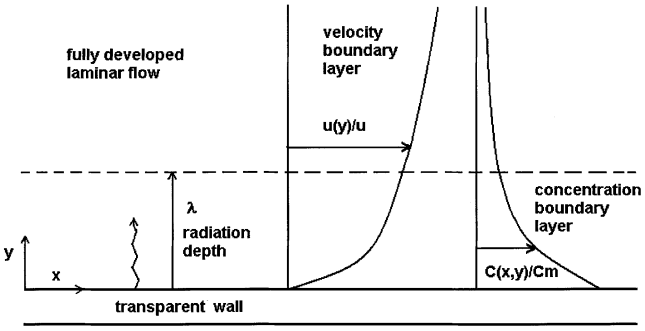

Figure 2. Velocity and concentration boundary layers and the radiation penetration depth.

The yield of the triiodide photoproduct is easily monitored by spectrophotometry at either 350 or 450 nm, depending on the concentration. The quantum yield of $\varphi = 0.75$ mol I_3/einstein is relatively constant with either temperature or reagent iodide concentrations (Rahn, 1999). With the addition of a borate buffer (pH 9.25) to minimize thermal oxidation, stock solutions of 0.6 M KI and 0.1 M KIO_3 with the borate buffer are stable and insensitive to ambient light in the visible spectrum.

Similitude

In the present study we assume a fully developed, laminar flow adjacent to a transparent wall, as shown in Figure 2. Below the quantities $C(I_3^-)$ and $C(x,y)$ represent the bulk and local molar concentrations, respectively, of the product triiodide. Since the absorbance of potassium iodide is large at a wavelength of 254 nm, we also assume that the product concentration is proportional to the number of photons absorbed or

$$C(I_3^-) = \gamma Cm \quad (5)$$

where $\gamma < 1$. Here the quantity Cm is the maximum triiodide concentration determined from the quantum efficiency of the photolysis reaction. Thus, one obtains

$$Cm = nI_o A_l \varphi/\alpha q \quad (6)$$

where n is the number of lamps and I_o, A_l are the intensity and irradiated area of each lamp, respectively. The remaining parameters in Eq. 6 are q the volume flow rate; $\varphi = 0.75$ mol triiodide/mol photons, which is the quantum efficiency; and $\alpha = 4.72 \times 10^5$ J/mol photons, which is the conversion factor from photons to energy.

The increase in product concentration now becomes

$$dC(I_3^-)/dx \quad \alpha \quad dCm/dx \quad (7)$$

where it is convenient from Eqs. 6 to define

$$dCm = I_{av} P_l \varphi dx/(\alpha q) \quad (8)$$

In Eq. 8 $I_{av} P_l L = nI_o A_l$, where I_{av} is the average intensity of the incident radiation over the irradiated perimeter length P_l and L is the irradiated channel length.

The change in the bulk concentration of product $C(I_3^-)$ must be proportional to the change in its local value $C(x,\lambda)$ within the concentration radiation boundary layer. Thus, from a mass balance

$$dC(I_3^-) \quad \alpha \quad dC(x,\lambda)P_l\mu_\lambda\lambda/q \tag{9}$$

where $u_\lambda = u(\lambda)$ is the fluid velocity at $y = \lambda$ in Figure 2, which is proportional to the average velocity in the radiation boundary layer. The concentration profile is now assumed to be self-similar in fully developed, laminar flow, that is, the local concentration profile $C(x,y)$ normalized with either the local average (or maximum) concentration is independent of the axial position within the channel, or

$$C(x,y)/Cm(x) \quad \alpha \quad f\left(y/A_c^{1/2}\right) \tag{10}$$

From Eq. 10, the change with axial position becomes

$$dC(x,\lambda)/dCm(x) \quad \alpha \quad f\left(\lambda/A_c^{1/2}\right) \tag{11}$$

where A_c is the cross-sectional area of the flow. Substituting Eq. 9 into Eq. 11, one obtains

$$dC(I_3^-)q/(\,dCm(x)P_lu_\lambda\lambda) \quad \alpha \quad f\left(\lambda/A_c^{1/2}\right) \tag{12}$$

Integrating Eq. 12 along the length of the reactor, the outlet concentration of product becomes

$$C(I_3^-)q/(P_lu_\lambda\lambda Cm) \quad \alpha \quad f\left(\lambda/A_c^{1/2}\right) \tag{13}$$

The characteristic fluid velocity within the concentration boundary layer u_λ is estimated to be

$$u_\lambda/u \quad \alpha \quad \lambda/\delta \tag{14}$$

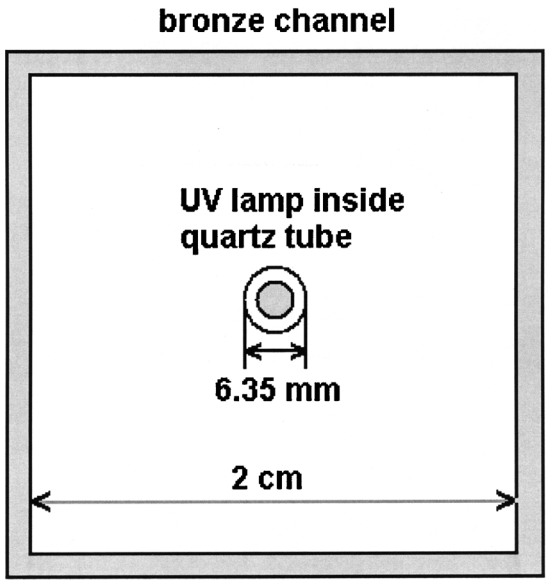

Figure 3. Cross section of square reaction channel.

Table 1. Reactor Dimensions (cm)

	Taylor–Couette $Ta = 0$	Taylor–Couette $Ta = 100$	Channel
P_l	12.9	12.9	2.0
P	23.5	23.5	10.16
A_c (cm^2)	3.9	3.9	3.9
d_h	0.668	0.668	1.52
δ	0.167	0.07	0.38

for $\lambda \le \delta$, where δ is the laminar film thickness (or in some cases, the boundary-layer thickness) as discussed below (Bird et al., 2002). Also, the fraction of irradiated perimeter P_l can be defined in the form

$$P_l/P = \beta \tag{15}$$

where P is the wetted perimeter of the reactor. Moreover, the volume flow rate $q = uA_c$, where the cross-sectional area of the flow $A_c = Pd_h$ in terms of the hydraulic diameter, d_h, and the total perimeter, P. Substituting Eqs. 14 and 15, one obtains a similarity law for the product in the form

$$C(I_3^-)d_h\delta/(\,\beta\lambda^2Cm) \quad \alpha \quad f\left(\lambda/A_c^{1/2}\right) \tag{16}$$

Experimental Apparatus

A solution of 0.6 M potassium iodide KI and 0.1 M potassium iodate KIO_3 buffered (pH 9.25) with borate was pumped through each of the two UV reactors described below. The absorbance of triiodide at the outlet was measured at either 350 or 450 nm, depending on the concentration of triiodide.

Channel

A continuous-flow reactor channel 18.5 cm in length was constructed from a bronze 2×2-cm-ID square. Centered in the channel was a fused-quartz capillary tube, as shown in the cross section of Figure 3. The quartz tube holds two cold-cathode, low-pressure, mercury UVC lamps for a total effective irradiated length of 13 cm. The intensity of the radiation for both lamps (wavelength ~ 254 nm) was 4 mW/cm^2, providing a total power input of 0.31 W.

The irradiated volume of the reactor was 56 mL, including two PVC flow straighteners at both ends, and was operated over a range of flow rates from $10 < q < 40$ mL/min. The reactor Reynolds number covered the range $6 < \mathrm{Re} < 25$ for the indicated flow rates, providing fully developed laminar flow in the cross-sectional area. The cross-sectional area of the channel is $A_c = 3.9$ cm^2 with a wetted perimeter $P = 10.2$ cm, a hydraulic diameter $d_h = 1.52$ cm, and an irradiated perimeter length $P_l = 2$ cm. These diameters are listed in Table 1 along with an estimate of the laminar film thickness of $\delta = d_h/4 = 0.38$ cm that corresponds to the distance to the center line of the asymmetric cross section.

Taylor – Couette

A Taylor vortex column, as shown in Figure 4, was constructed, consisting of a bronze rotor 3.43 cm in diameter by

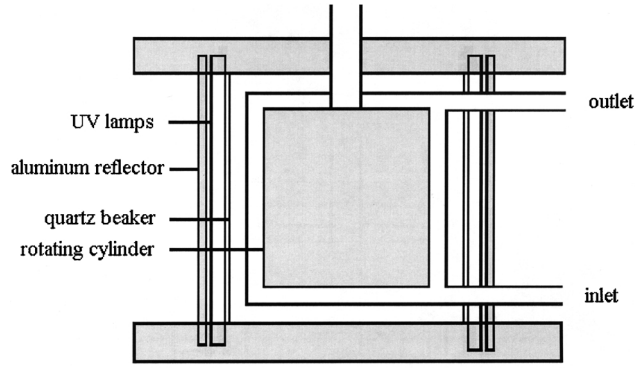

Figure 4. Annular gap reactor: rotation of inner cylinder produces Taylor–Couette flow.

5 cm in length centered within a fused-quartz beaker, with an inside diameter of 4.1 cm providing an annular gap width of $d = 0.334$ cm (Forney and Pierson, 2003). The irradiated holdup volume was 12 mL with a range of flow rates between $10 < q < 40$ mL/min. Four cold-cathode, low-pressure mercury UVC lamps with effective lengths of 3.1 cm were positioned around the quartz beaker, as shown in Figure 5. The lamps were surrounded by an aluminum reflector with an over 90% reflectivity of UV radiation at a 254-nm wavelength (Incropera and Dewitt, 1996). The intensity of radiation for each lamp (wavelength ~ 254 nm) was rated at 4 mW/cm^2, providing a range of power input from 0.078 W to 0.31 W depending on the number of lamps engaged (Gilway Technical Lamps, Catalog No. 169, 2001). The angular rotation of the rotor was controlled by a permanent-magnet DC motor between $0 <$ rpm < 75, providing a Taylor number covering the range $0 < Ta < 200$ where $Ta = Ud(d/R)^{1/2}/\upsilon$. Here, d is the gap width, R is the rotor radius, $U = \omega R$ is the rotor surface velocity, and υ is the kinematic viscosity of the fluid.

It should be noted that both of the reactors were constructed with the same cross-sectional areas of 3.9 cm^2, and that both have similar material surfaces (bronze) that reflect the UV radiation so that differences in surface radiation absorptivities are minimized. Moreover, with all four lamps engaged in the Taylor column, the photon input is identical in both reactors for roughly equal volume flow rates.

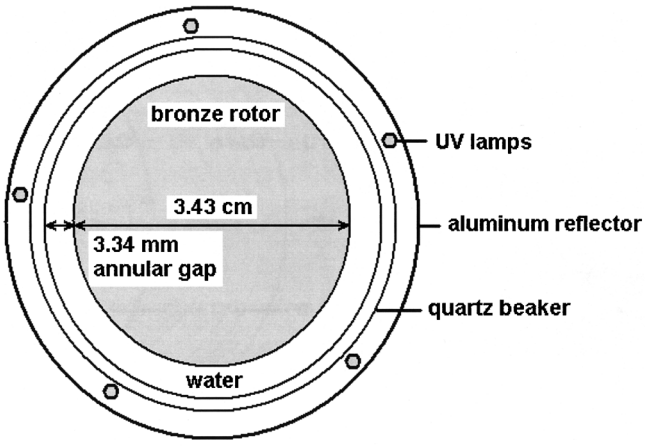

Figure 5. Cross section of annular gap reactor.

Radiation penetration depth

Since the solution absorbance is defined by

$$A = \lambda \epsilon C \tag{17}$$

where the intensity of radiation is $I/I_o = 10^{-A}$, ϵ is the extinction coefficient, C is the absorbing species, and λ is the radiation depth. The reaction layer is, therefore, confined to a layer

$$\lambda \quad \alpha \quad 1/\epsilon C \tag{18}$$

as shown in Figure 2. Since the absorbance $A = \lambda \epsilon C_i(I)$ is 200 for a 0.6 M KI and 0.1 M KIO_3 solution, the extinction coefficient at a wavelength of 254 nm was calculated to be $\epsilon = 333\ \mathrm{M^{-1}cm^{-1}}$ (Rahn, 1999). Setting the absorbance $A = 1$ that represents a radiation depth over which 90% of the UV photons are absorbed, one calculates the radiation depth to be $\lambda = 1/\epsilon C_i(I)$.

Laminar film thickness

The laminar film thickness corresponds to the distance to the center line for steady flow in a channel. In the case of flow through the Taylor column at zero rpm or $Ta = 0$, the center line is located at the center of the annual gap or $\delta = d_h/4 = 0.167$ cm, where d_h is defined for concentric cylinders. Recall in the discussion of the channel flow earlier that the same quantity, $d_h/4$ was also chosen for the laminar film thickness.

When the Taylor column is operated with laminar vortices at $Ta > 41$, the laminar film thickness is interpreted as the laminar boundary layer. In this case (Baier et al., 1999; Forney and Pierson, 2002)

$$\delta \quad \alpha \quad d_h/Ta^{1/2} = 0.07\,\mathrm{cm} \tag{19}$$

for a Taylor number of 100, as shown in Table 1.

Results and Discussion

A solution of 0.6 M potassium iodide (KI) and 0.1 M potassium iodate (KIO_3) buffered (pH 9.25) with borate was pumped through the Taylor column at 16.5 mL/min. The absorbance of triiodide at the outlet was measured at 450 nm with four lamps engaged (0.31 W). The rpm of the rotor, controlled by a permanent-magnet DC motor, was varied between $0 <$ rpm < 120, providing a Taylor number covering the range $0 < Ta < 300$. The triiodide concentration shown in Figure 6, as expected, clearly indicates a large increase of roughly 70% for Taylor numbers $Ta > Ta_c$, where the lower limit of $Ta_c \sim 41$ corresponds to the onset of Taylor vortices at low axial Reynolds numbers. Since the cross-sectional area for the flow within the annular gap is 3.9 cm^2, the axial Reynolds number was $Re_x < 10$ for all experiments, and, thus, had no effect on the critical Ta_c (Schlichting, 1979).

The same solution as just given was pumped through both the channel and Taylor column where the latter was operated at a Taylor number $Ta =$ 100 for a range of flow rates as indicated in Figure 7. These data correspond to a single run where the indicated scatter was due to variations in fluid

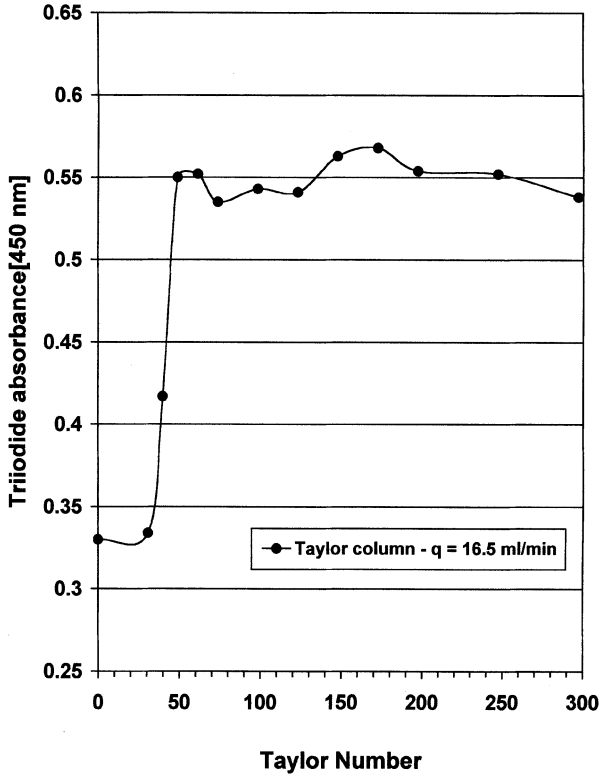

Figure 6. Triiodide absorbance vs. Taylor number.

Inlet aqueous concentrations of 0.6 M KI and 0.1 M KIO_3.

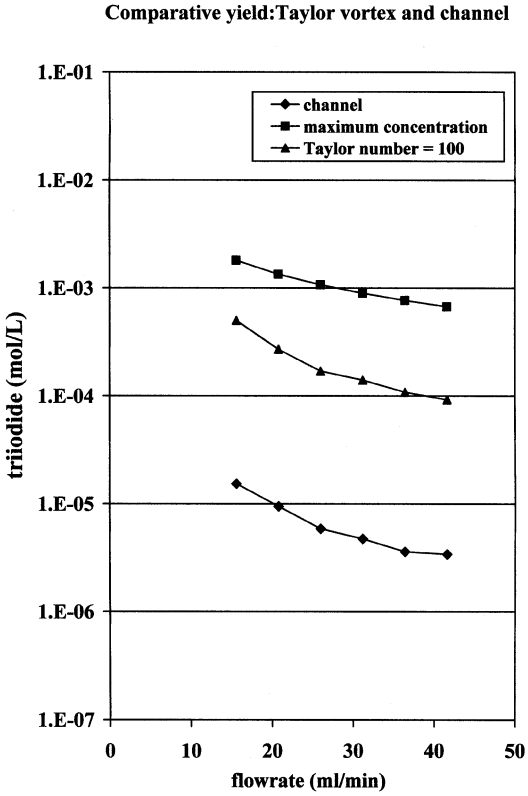

Figure 7. Triiodide yield vs. flow rate.

Inlet aqueous concentrations of 0.6 M KI and 0.1 M KIO_3. *Cm* is maximum concentration calculated from the product of photon dose and quantum efficiency.

flow rates of up to 10% around the small values of 15 mL/min. Also shown is the maximum concentration, C_m for both reactors with a maximum power input of 0.31 W in each case. The increase by a factor of roughly 35 for the Taylor column compared to the channel is the result of a favorable increase in the irradiated surface-to-volume ratio for the Taylor column and the reduction in the boundary-layer thickness, as discussed below. The product yield for the Taylor column, however, is roughly 37% of the yield computed from the product of photon dosage and quantum efficiency due to scattering and absorption of incident radiation and to the back reaction of the form (Dainton and Logan, 1965)

$$e_{aq}^{-} + I^{-}{}_3 \rightarrow I_2^{-} + I^{-} \tag{20}$$

The concentrations of the product triiodide are replotted in Figures 8 and 9 as a function of the maximum photon input converted to units of moles triiodide per liter by the quantum efficiency for the reaction. For fixed geometry and photon input, one can assume average properties across the reactor and integrate the expression

$$udC/dx = r \tag{21}$$

where the average rate constant [mol/L-s]

$$r \quad \alpha \quad nI_0 A_l \varphi/\alpha V \tag{22}$$

and V is the irradiated volume of the fluid. Thus, the concentration of triiodide formed from Eq. 21 with $dx/u = dV/q$ is

$$C(I_3) = \gamma rV/q = \gamma Cm \tag{23}$$

Here, the factor $\gamma < 1$ must account for both the loss of input photons to liquid and surface absorption, the effects of back reactions of the type in Eq. 20, and importantly, the geometry of the reactor and lamp configuration. The latter would account for nonuniform radiation levels and the effects of the hydrodynamics, namely, velocity and concentration boundary layers. The advantage of geometries that provide liquid surface renewal near the irradiated surfaces are clearly superior since $\gamma = 0.01$ for the channel, but increases to $\gamma = 0.37$ for the Taylor column in the presence of laminar vortices for fixed $Ta = 100$. The conditions for maximum γ or optimum photoefficiencies are discussed in the earlier work of Forney and Pierson (2003).

Triiodide absorbance in both the channel and Taylor column was measured in Figure 10 for a range of inlet iodide concentrations. Also included are values for the Taylor column at zero rotation, where the latter corresponds to a channel flow through an annular gap, shown in Figure 4 with a markedly different geometry and lamp configuration than the square channel of Figure 3.

The radiation penetration depth $\lambda \ \alpha \ 1/C$ for any photolytic reactor, where C is the reactant absorbing species. Thus, one observes a rapid, nearly linear, increase in product

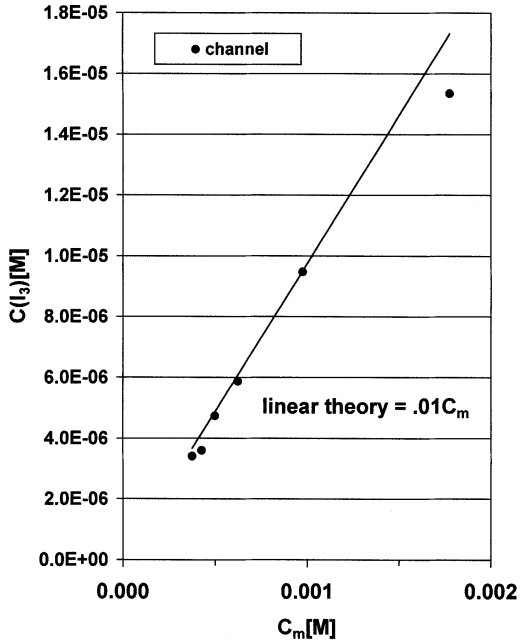

Figure 8. Triiodide yield in square channel vs. maximum concentration *Cm* based on photon dose; data from Figure 7.

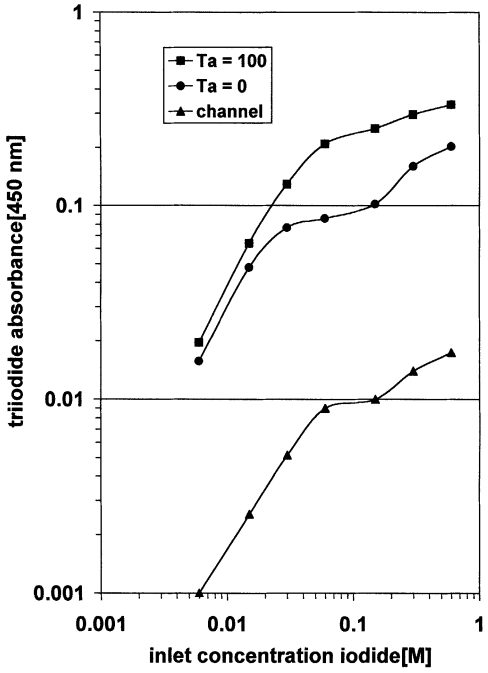

Figure 10. Outlet triiodide absorbance vs. inlet iodide concentration for all three reactors.

concentration in Figure 10 for small concentrations of inlet iodide. For larger values of inlet iodide, however, the increase in the product is clearly reduced, suggesting a transition in the order of the reaction kinetics.

The data in the present study are plotted in Figure 11 as a universal curve, as suggested by the proposed similarity law of Eq. 16. The dimensionless of triiodide concentration has a slope of -2 (least-square value of -2.3) for large reactant concentration or

$$C(I_3^-)\,d_h\,\delta/(Cm\,\beta\lambda^2) \quad \alpha \quad A_c/\lambda^2 \tag{24}$$

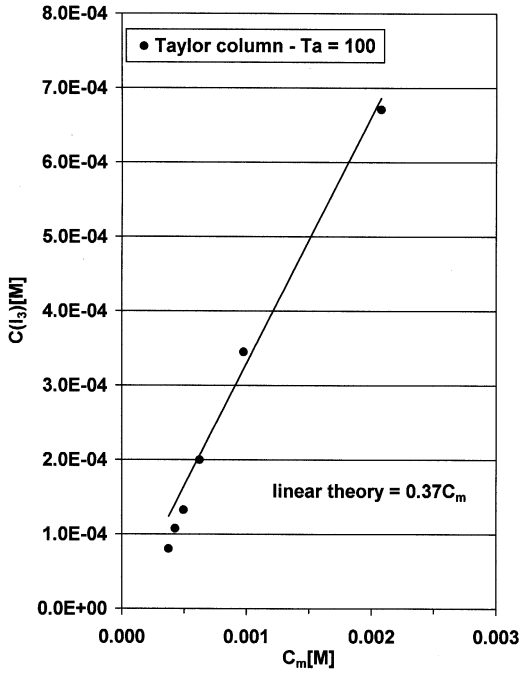

Figure 9. Triiodide yield in Taylor–Couette flow vs. maximum concentration based on photon dose; data from Figure 7.

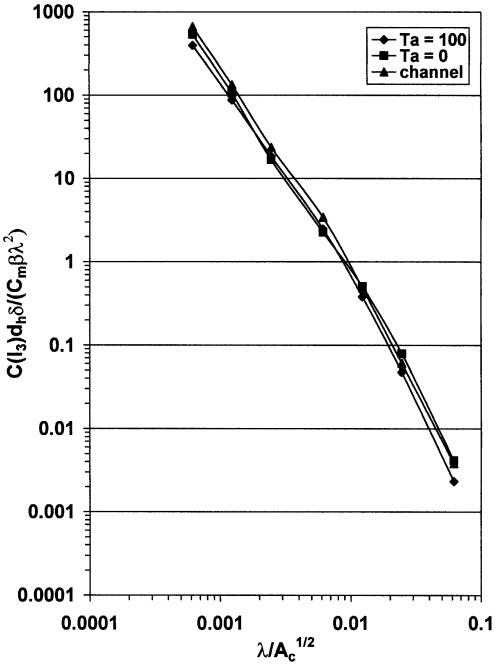

Figure 11. Normalized yield of triiodide vs. radiation penetration depth for all three reactors.

for $\lambda/A_c^{1/2} < 0.01$. Under these conditions the product concentration is large within the relatively thin reaction layer defined by the radiation penetration depth, λ. Moreover, $C(I_3^-)$ is independent of the absorbing reactant species, since the parameter $\lambda \alpha 1/C(I^-)$ cancels out of Eq. 24, suggesting that the reaction kinetics are roughly zero order. Physically, since the product triiodide is large, diffusion limitations for I_3^- and the solvated electron would promote the back reaction of Eq. 20.

The dimensionless concentration of the triiodide product has a slope of -3 (least-square value of -3.06) on the right of Figure 11 for small absorbing reactant concentrations or

$$C(I_3^-)\, d_h \delta/(Cm\beta\lambda^2) \quad \alpha \quad A_c^{3/2}/\lambda^3 \qquad (25)$$

for $\lambda/A_c^{1/2} > 0.01$. Under these conditions the product concentration is uniform across the reactor and the reaction kinetics are first order with respect to the reactant-absorbing species.

In either case, that is, large or small reactant concentrations, the product yield is larger for system designs with small velocity boundary layers δ, small hydraulic diameters d_h (or large area-to-volume ratios), and with a large fraction of the reactor perimeter β irradiated.

Conclusions

A similarity law is proposed for the yield from laminar photolytic reactors. In particular, the yield from a fast photolytic reaction is considered in the following three distinctly different reactor geometries: a square channel, an annular gap between concentric cylinders, and Taylor–Couette flow. The similarity law, based on the assumption of a self-similar product concentration profile, demonstrates that the reaction rate can best be described with either zero (small λ) or first-order (large λ) kinetics. Here, the distinction between both cases is determined by the radiation penetration depth λ.

The proposed scaling law is valid for solutions in which the radiation penetration depth is less than (or equal) to the laminar film thickness. In this case the solutions have a large absorbance and the effect of hydrodynamics near the transparent wall is important. Of the three geometries considered, the Taylor–Couette flow ($Ta > Ta_c$) is superior where Ta_c is the critical Taylor number for the onset of laminar vortices. The latter geometry is analogous to flow perpendicular to a tube bank.

In comparison, the annular gap produced a factor of 10 more product than the square channel. Moreover, the Taylor–Couette flow produced from two to three times more product than the annular gap. Independent of either geometry or inlet concentration, however, the product yield is larger for system designs with small-velocity boundary layers, δ, small hydraulic diameters, d_h (or large area-to-volume ratios), and with a large fraction of the reactor perimeter, β, irradiated.

Acknowledgment

The work was supported by FoodPAC from Georgia's Traditional Industries Program for Food Processing under contract GTRI #N-5430-200. The authors acknowledge useful discussions concerning the Taylor vortex column with Mr. Richard Holl from Holl Technologies Inc.

Notation

A = absorbance
A_c = cross-sectional area to flow, cm
A_l = single UV lamp area, cm^2
C = bulk iodide or triiodide concentration, mol/L
$C(x,y)$ = local triiodide concentration, mol/L
Cm = maximum triiodide from all photons, mol/L
d = gap width, cm
d_h = hydraulic diameter ($= A_c/P$), cm
I = radiation intensity, W/cm^2
I_{av} = average radiation intensity, W/cm^2
I_o = initial radiation intensity, W/cm^2
n = number of lamps
P = wetted perimeter of reactor, cm
P_l = irradiated perimeter of reactor, cm
q = volume flow rate, mL/min
r = rate constant, mol/L-s
R = radius of rotating cylinder, cm
Ta = Taylor number
Ta_c = critical Taylor number for laminar vortices
u = mean axial fluid velocity, cm/s
u_λ = axial fluid velocity in radiation boundary layer, cm/s
V = reactor holdup volume (irradiated), mL
x = axial position in reactor, cm
y = position perpendicular to transparent wall, cm

Greek letters

α = conversion factor, 4.72×10^5 J/einstein
β = nondimensional factor
γ = nondimensional factor
ϵ = extinction coefficient, $M^{-1} \cdot cm^{-1}$
δ = laminar film or velocity boundary-layer thickness, cm
λ = radiation penetration depth, cm
ω = angular velocity of cylinder, rad/s
φ = quantum efficiency, 0.75 mol triiodide/Einstein

Literature Cited

Baier, G., T. M. Grateful, M. D. Graham, and E. N. Lightfoot, "Prediction of Mass Transfer in Spatially Periodic Systems, *Chem. Eng. Sci.*, **54**, 343 (1999).

Bird, R. B., W. E. Stewart, and E. N. Lightfoot, *Transport Phenomena*, 2nd ed., Wiley, New York (2002).

Blatchley, E. R., III, W. L. Wood, and P. Schuerch, "UV Pilot Testing: Intensity Distribution and Hydrodynamics," *J. Environ. Eng., ASCE*, 258 (1995).

Blatchley, E. R., Z. Do-Quang, M. L. Janex, J. M. Laine, "Process Modeling of Ultraviolet Disinfection," *Water. Sci. Tech.*, **28**, 63 (1998).

Chiu, K., D. A. Lyn, P. Savoye, and E. R. Blatchley III, "Integrated UV Disinfection Model Based on Particle Tracking," *J. Environ. Eng.*, **125**, 7 (1999).

Congdine, D. M., ed., *Van Nostrand's Scientific Encyclopedia*, 5th ed., Van Nostrand Reinhold, New York, p. 1764 (1976).

Cortelyou, J. R., Effects of Ultraviolet Irradiation on Large Populations of Certain Water-Borne Bacteria in Motion," *Appl. Microbiol.*, **2**, 227 (1954).

Dainton, F. S., and S. R. Logan, "Primary Process in the Photolysis of the Iodide Ion in Aqueous Solution, *Proc. R. Soc. London*, **287**, 281 (1965).

Forney, L. J., and J. A. Pierson, "Optimum Photolysis in Taylor–Couette Flow," *AIChE J.*, **49**, 727 (2003).

Incropera, F., and D. Dewitt, *Introduction to Heat Transfer*, 3rd ed., Wiley, New York (1996).

Jagger, S. M., *Introduction to Research in Utraviolet Photobiology*, Prentice Hall, Englewood Cliffs, NJ (1967).

Janex, M. L., P. Savoye, Z. Do-Quang, E. R. Blatchley, III, and J. M. Laine, "Impact of Water Quality and Reactor Hydrodynamics on

Wastewater Disinfection by UV, Use of CFD Modeling for Performance Optimization," *Water. Sci. Techol.*, **38**, 71 (1998).
Luckiesh, M., and L. L. Holladay, "Disinfecting Water by Means of Germicidal Lamps," *Gen. Electr. Rev.*, **47**, 45 (1944).
Lyn, D. A., K. Chiu, and E. R. Blatchley, III, "Numerical Modeling of Flow and Disinfection in UV Disinfection Channels," *J. Environ. Eng.*, **125**, 17 (1999).
Miller, R. L., A. G. Fredrickson, A. H. Brown, and H. M. Tsuchiya, "Hydromechanical Method to Increase Efficiency of Algal Photosynthesis," *Ind. Eng. Chem. Process Des. Dev.*, **3**, 134(1964).
Ollis, D. F., and C. S. Turchi, "Heterogeneous Photocatalysis for Water Purification," *Environ. Prog.,* **9**, 229 (1990).
Oliver, B. G., and E. G. Cosgrove, "The Disinfection of Sewage Treatment Plant Effluents Using Ultraviolet Light," *Can. J. Chem. Eng.*, **53**,170 (1975).
Oster, G. K., and N. Yang, "Photopolymerization of Vinyl Monomers," *Chem. Rev.*, **68**, 125 (1968).
Rahn, R. O., "Potassium Iodide as a Chemical Actinometer for 254 nm Radiation: Use of Iodate as an Electron Scavenger," *Photochem. Photobiol.*, **66**, 450 (1997).
Rahn, R. O., P. Xu, and S. L. Miller, "Dosimetry of Room-Air Germicidal (254 nm) Radiation Using Spherical Actinometry," *Photochem. Photobiol.*, **70**, 314 (1999).
Scheible, O. K., "Development of a Rationally Based Design Protocol for the Ultraviolet Disinfection Process," *J. Water Pollut. Control Fed.*, **59**, 25 (1987).
Schlichting, H, *Boundary Layer Theory*, 7th ed, McGraw-Hill, New York (1979).
Sczechowskii, J. G., C. A. Koval and R. D. Noble, "A Taylor Vortex Reactor for Heterogeneous Photocatalysis," *Chem. Eng. Sci.*, **50**, 3163 (1995).
Severin, B. F., M. T. Suidan, B. E. Rittmann, and R. S. Engelbrecht, "Inactivation Kinetics in a Flow-Through UV Reactor," *J. Water Pollut. Control Fed.*, **56**,164 (1984).
Taylor, G. I., Stability of a Viscous Liquid Contained Between Two Rotating Cylinders," *Phil. Trans. R. Soc. London A*, **223**, 289 (1923).

Manuscript received June, 19, 2002, and revision received Dec. 11, 2002.